Ferrite-Less Circular Pad With Controlled Flux Cancelation for EV Wireless Charging

Abiezer Tejeda, *Member, IEEE*, Claudio Carretero, *Senior Member, IEEE*, John T. Boys, and Grant A. Covic, *Senior Member, IEEE*

***Abstract*—In this paper, a new ferrite-less wireless charging pad, called circular nonferrite pad, for roadway applications is introduced. The pad is characterized by having the ability to control leakage flux to reduce the electromagnetic fields outside the charging region. In addition, the pad shows low sensitivity to changes in the self-inductance due to secondary pad misalignment. A comparison of this new pad with similar-sized ferrite pads and single spiral couplers is presented. A formal mathematical description of the pad is shown here with finite element method simulations along with lab measurements to verify the validity of the models. The costs, advantages, and limitations of the new pad are also investigated.**

***Index Terms*—Electric vehicles (EVs), electromagnetic field (EMF) shielding, inductive power transfer (IPT), leakage flux, nonferrite, two-coil resonator.**

I. Introduction

INDUCTIVE power transfer (IPT) is a rapidly growing technology that enables energy to be transferred wirelessly between one or more electrical systems. Common applications range from clean rooms, factory automation, transportation, lighting, wireless sensors, and consumer electronics devices to transcutaneous implantable devices [1]–[10].

Wireless charging is not only convenient but also safe, robust, reliable, and especially suitable for applications in harsh, wet or dusty environments where mechanical contact can be detrimental to the electrical system itself. More recently, the automobile industry has been in the process of developing standards for IPT systems to enable electric vehicles (EVs) to be charged wirelessly, both while stationary and in motion [11]–[16]. Over the years, different magnetic pads have been developed that can couple power over relatively large air gaps. These pads are commonly named according to the geometry of the coil and/or the way the magnetic field is generated. Among the most notable are the circular (CP), double D (DD) and its variant with a quadrature coil DDQ, bipolar (BPP), solenoid, and tripolar (TPP) pads [14], [17]–[23]. Some pads are further classified as polarized (examples include the DD and Solenoid) or nonpolarized (the CP or square shaped pads) depending on the path taken by the magnetic field, while the DDQ, BPP, and TPP can generate either polarized or nonpolarized fluxes depending on the phases of the currents flowing through the different coils in the primary.

High power is needed to provide the energy required by EVs and to decrease the battery charging time, which occurs over relatively large air gaps. In consequence, strong electromagnetic fields (EMF) are generated in and around the charging region of the pads. In consumer applications, e.g., EV charging, safety regulations must be met to keep EMF levels within the safety guidelines for human exposure [24]–[26]. Several shielding methods have been devised and utilized in the past to suppress undesired EMFs including both active and passive shielding [27]–[38]. This paper introduces a magnetic coupler suitable for roadway charging applications with the ability to reduce stray magnetic leakage fields using active cancelation techniques.

Roadway pads must be designed to have not only excellent electrical and magnetic performance, but they also must be integrated into existing infrastructure and be extremely rugged to survive under the extreme forces and vibrations under roads. In addition, they must require minimal maintenance, be cost effective, interoperable, and flexible to adapt to fast changing technologies. In order to meet most or all of these requirements, the materials used for the charging pads must be carefully selected, designed, and tested. Roadway pads today use, among others, aluminum and plastic as shielding and protective materials, respectively. However, these materials may not survive or integrate easily with existing roadway technology, and might degrade over time, thereby changing the pad's ability to transfer power adequately and efficiently. Furthermore, if robust protective materials are not used, the brittle and expensive ferrite used to boost power transfer and control the leakage of IPT pads can be exposed to the elements and its performance might be compromised [39]. In addition to these mechanical issues, at high power, the losses in core and shielding materials can become significant [40]. Another practical consideration is thermal runaway in high-power IPT systems. Traditional cooling methods may be difficult to implement under the roadway, and high temperatures can also compromise or cause deterioration of the entire system.

Ferrite-less pads for EV charging applications have been recently proposed in the literature as alternative pads with

Manuscript received June 28, 2016; revised October 12, 2016; accepted December 6, 2016. Date of publication December 20, 2016; date of current version June 23, 2017. This work was supported in part by the Spanish Ministry of Education, Culture, and Sports under Grant CAS15/00094. Recommended for publication by Associate Editor S. Williamson.

A. Tejeda, J. T. Boys, and G. A. Covic are with the Department of Electrical and Computer Engineering, The University of Auckland, Auckland 1010, New Zealand (e-mail: atej217@aucklanduni.ac.nz; j.boys@auckland.ac.nz; ga.covic@auckland.ac.nz).

C. Carretero is with the Department of Fisica Aplicada, Universidad de Zaragoza, Zaragoza 50018, Spain (e-mail: ccar@unizar.es).

Color versions of one or more of the figures in this paper are available online at http://ieeexplore.ieee.org.

Digital Object Identifier 10.1109/TPEL.2016.2642192

increased mechanical robustness are suitable for roadway applications [38], [39], [41]–[45]. In [38], active coils driven out of phase were added to both the primary and secondary pads to mitigate the EMF outside the desired region of charging. In [43], it was found that a combination of a canceling *LC*-resonant coil and a conductive plate is a good candidate for controlling the leakage flux in ubiquitous large air-gap applications. The EMF of the main coil can be either enhanced or reduced depending on whether an *LC*-resonant coil is below or above resonance, respectively, which requires a precise matching of the resonant network to achieve a good performance. This paper explores a similar system using only an inductive canceling coil connected in a series-opposing configuration with the main coil and designed so that most of the magnetic field under the pad and outside the charging area is minimized. The series-opposing configuration enforces the same current level in both the main coil and canceling coil but in opposing phase; thus, the field cancelation is only controlled by the geometry of the system.

This paper investigates a primary pad having a structure similar to a two-coil system (although wound as a single winding) comprising a main flux producing coil and a lower canceling coil, suitable for high-power roadway EV charging. This pad is hereafter referred to as a circular nonferrite pad (CNFP). This structure is based on initial proposals detailed in [46] but is now reported for the first time in the academic literature with additional analysis. A similar system with some remarkable differences has been recently proposed in [44]. In [44], a low-power system is proposed and analyzed with the cancelation coil, called parasitic coil, in a short-circuit condition. Leakage was measured along a reference line on the underside of the pad and the axial component of the magnetic field B_z was measured. The pad in [44] is suitable for low-power applications, e.g., biomedical implants. The work in [46] and described in this paper investigates a high-power system for roadway charging applications. It takes into account the tradeoffs between a low undesired magnetic leakage field, minimal impact in power transfer capability, and minimum copper usage by optimizing the amp-turns ratio between the main and canceling coils and using an active canceling coil that is wound in a series-opposing configuration.

The CNFP resembles the geometry of Helmholtz coils commonly used in the biomedical field for wireless charging of implantable devices, such as endoscopic capsules [47]–[49]. However, it is worth pointing out several important distinctions between the two. First, the power levels and coupling factors for biomedical applications are very small and impractical for EV charging applications. Second, Helmholtz coils are characterized by uniformity of the magnetic field in the region between the two coils, for which the use of identical coils (same size and number of turns), separated by a distance equal to the radius of the coils, are required. In contrast, here the coils of the CNFP have a different number of turns and different radii and the distance between the coils is not necessarily equal to the radius of either coil. Finally, the CNFP aims to reduce undesired flux in the regions under the canceling coil and outside the charging area where humans may be present, with minimal impact to the flux out the top of the pad. Uniformity of the magnetic flux density between the two coils is not a design objective.

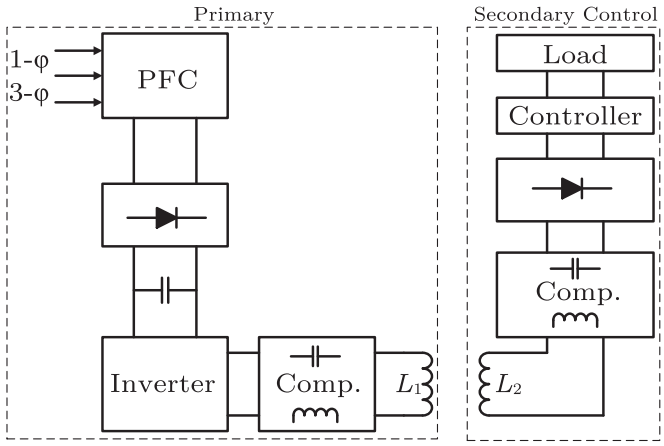

Fig. 1. General IPT system overview.

This paper is organized as follows. Section II provides a general overview of IPT systems. Section III gives a mathematical analysis of the proposed pad. In Section IV, the CNFP is introduced. It is shown to be able to produce a one-side flux with reduced emissions by virtue of active magnetic shielding. The pad is further analyzed in Section V to optimize its power transfer capability in terms of coupling factors and leakage emissions. In Section VI, the results of FEM simulations are validated by lab measurements. Finally, in Section VII, a summary of the findings is provided.

II. Wireless Power Transfer Systems

A simple IPT system, as shown in Fig. 1, comprises two inductive coils L_1 and L_2, with mutual inductance M; the primary inductor L_1 is driven by current I_1 at an operating angular frequency ω to generate an alternating magnetic field. Using a conventional analysis, a voltage is induced in a secondary coil L_2 when it is immersed in this variable magnetic field. The induced open-circuit voltage in L_2 is given by $V_{\rm oc} = j\omega M I_1$ and the short-circuit current in the secondary coil is $I_{\rm sc} = MI_1/L_2$.

The maximum output power that can be transferred is given by the product of the open-circuit voltage $V_{\rm oc}$, the short-circuit current $I_{\rm sc}$, and the secondary loaded quality factor Q_2 of the secondary circuit as expressed below [11]

$$P_{\rm out} = V_{\rm oc} I_{\rm sc} Q_2 \tag{1}$$

which can be expressed as

$$P_{\rm out} = \omega L_1 k^2 I_1^2 Q_2 = k^2 V_1 I_1 Q_2 \tag{2}$$

where $k = M/\sqrt{L_1 L_2}$ is the coupling factor, which constitutes a measure of the ratio between the magnetic flux of the secondary with respect to the total magnetic flux generated by the primary ω is the operating angular frequency, and $P_{\rm su} = V_{\rm oc} I_{\rm sc}$ is the uncompensated apparent power at the secondary. For an increase in power, either the input VA_1 $(V_1 I_1)$, Q_2, or k has to be increased. However, increasing the primary VA increases the cost and, although it can be limited by adding extra series

capacitance to lower the VA seen by the power supply, the tuning sensitivity and costs are increased [11]. There are also practical limits to increasing Q_2 because the efficiency is lowered due to high circulating currents in the secondary resonant tank and the system becomes more difficult to control and more sensitive to secondary coil displacements. Increasing the power by improving the magnetic coupling factor k is the optimal solution as it is a good tradeoff between efficiency and total cost [4].

Conventionally, magnetic materials are used to increase the coupling coefficient by providing a low reluctance path to shape the flux. In addition, the geometry of the coil plays an important role in increasing the performance of the system as well as containing the flux within the desired region of charging. This paper focuses on the latter method by proposing a circular pad with a one-sided field generated using a flux cancelation technique. Optimal design of the coil is considered to balance the tradeoffs, with a complete absence of magnetic materials.

Electromagnetic theory is commonly used to describe the magnetic field produced by different coils, for example, circular and square coils. The Biot–Savart law is a simple equation to find the axial field component of a loop coil. Using linear superposition, it can also be used to find the total flux density produced by the combination of several coils composed of multiple spiral turns. For instance, Helmholtz coils comprise two identical circular coils placed symmetrically along a central axis separated by a distance h that is equal to the radius of the coils, to produce an almost homogeneous magnetic field in the region between the two coils [50], [51]. Normally, the coils are connected in a series-aiding configuration. If the currents are 180° out of phase, then the configuration is called antiparallel Helmholtz coils with the effect of canceling the magnetic field in the center of the coils. The resultant magnetic field on the z-axis of the combined out-of-phase coils $B_1 + B_c$ can be expressed as

$$\begin{aligned} B_z &= B_1 + B_c \\ &= \frac{\mu_0 r^2}{2}\left[\frac{N_1 I_1}{\left(r_1^2 + z^2\right)^{3/2}} - \frac{N_c I_2}{\left[r_c^2 + (z+h)^2\right]^{3/2}}\right] \end{aligned} \tag{3}$$

where B_1 is the magnetic field arising from the main or top coil with N_1 turns and B_c is the magnetic field from the bottom coil with N_c turns as shown in Fig. 2(a). r_1 and r_c are the radii of the main and canceling coils, respectively.

It can be observed that by choosing appropriately the NI product, the radii r_1 and r_c, and h, a good balance can be found to minimize the leakage flux out the back of the pad, as seen in Fig. 2(b). Fig. 2(b) covers a range of combinations from an air coil, labeled as "No Cancelation," to two identical coils connected in a series-opposing configuration. The z component of the magnetic flux field B_z for different values of N_c with $\mathrm{OD}_1 = \mathrm{OD}_c = 500$ mm, $\mathrm{ID}_1 = \mathrm{ID}_c = 357.2$ mm, $h = 200$ mm, and $N_1 = 9$ is shown in Fig. 2(b) for each combination. For example, given a primary coil of radius r_1 with $N_1 I_1$ amp-turns, a canceling coil of the same radius can be designed by finding the right $N_c I_c$ and h to completely cancel the flux at a distance z along the center axis.

A front-to-back ratio (FBR) can be defined as the ratio of the area under the B_z curve on the top of the pad over the area under the B_z curve under the bottom side of the pad, as

$$\mathrm{FBR} = S_{\mathrm{top}}/S_{\mathrm{bottom}} \tag{4}$$

where $S_{\mathrm{top}} = \int_{z=0}^{\infty} B_z dz$ and $S_{\mathrm{bottom}} = \int_{z=-h}^{-\infty} B_z dz$. The FBR provides an indication of the ability of the pad to minimize the EMF in the region below the pad (under the cancelation coil). In Fig. 2(b), a maximum $\mathrm{FBR} = 20.844$ is found for the combination $N_1/N_c = 9/3$, while the minimum $\mathrm{FBR} = 0.740$ is found for $N_1/N_c = 9/5$. This is the situation specifically for the field along the axis, but (3) does not provide a complete picture of the overall flux density in the space surrounding the two coils and a more complex equation involving elliptic integrals is needed to give a better approximation, as is shown in Section III.

III. Mathematical Formulation of Model

Circular loop coils have been extensively a subject of study for the development of IPT systems due mostly to their simplicity for analysis and manufacturing as well as good magnetic and electrical properties. Different arrangements of multiple ferriteless circular coils for IPT were presented in [52] and [53], where a sound analysis and evaluation of the characteristics of such systems at low power was presented. In [54], a list of analytical formulae for inductance calculations of different coil shapes are given. The magnetic and electric fields of circular loops are well known and can be calculated using well-established methods. The radial $B_\rho(\mathbf{r}')$ and axial $B_z(\mathbf{r}')$ components of the magnetic field generated by a circular loop of radius ρ_i placed in the xy plane (with normal unit vector $\hat{\mathbf{z}}$) at a given z position, when carrying a current I_i can be found as [55]

$$\begin{aligned} B_\rho(\mathbf{r}') &= \mu_0 I_i \\ &\cdot \frac{(z'-z_i)\,k'\left[\left(2-k'^2\right)\mathbf{E}(k') - 2\left(1-k'^2\right)\mathbf{K}(k')\right]}{8\pi\left(1-k'^2\right)\sqrt{\rho_i \rho'^3}} \end{aligned} \tag{5}$$

$$\begin{aligned} B_z(\mathbf{r}') &= \mu_0 I_i k' \\ &\cdot \frac{\left[k'^2\left(\rho_i^2 - \rho'^2 - (z'-z_i)^2\right)\mathbf{E}(k') + 4 r_i r'\left(1-k'^2\right)\mathbf{K}(k')\right]}{16\pi\left(1-k'^2\right)\sqrt{(\rho_i \rho')^3}} \end{aligned} \tag{6}$$

where k' is defined as following:

$$k' = \sqrt{\frac{4\rho_i \rho'}{(\rho_i + \rho')^2 + (z'-z_i)^2}}. \tag{7}$$

The mutual inductance between two concentric spiral coils of radii ρ_i and ρ_j in air can be calculated as [56]–[58]

$$M_{ij} = \frac{\mu_0}{k'_{ij}}\sqrt{\rho_i \rho_j}\left[\left(2-k'^2_{ij}\right)\mathbf{K}\left(k'_{ij}\right) - 2\mathbf{E}\left(k'_{ij}\right)\right]. \tag{8}$$

Equation (8) provides a divergent result in terms of elliptic integrals for the self-inductance ($i = j$) of a closed-loop coil. However, an approximated expression is proposed by some authors for a closed-loop turn with cross section diameter d_i [56]

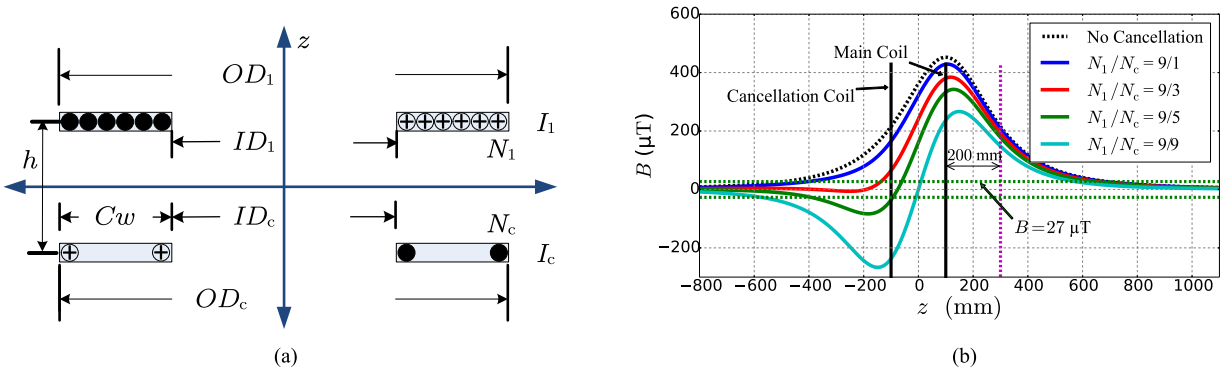

Fig. 2. Cross-sectional depiction and 2-D axial field plot of the CNFP. (a) Cross-sectional geometric parameters. (b) Axial component B_z of the magnetic field for different turns ratios between the main and cancelation coils keeping all other geometric parameters (h, OD$_c$, etc.) constant.

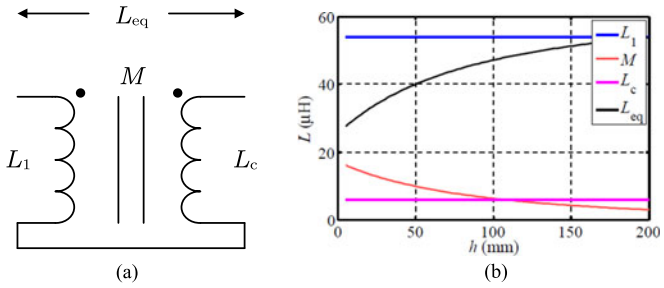

Fig. 3. (a) Equivalent circuit diagram of a CNFP pad. (b) Plots of analytical inductances and mutual inductance for a CNFP system.

TABLE I
CIRCULAR NONFERRITE PAD PARAMETERS

Parameter	Description	Value
L_{eq}	CNFP Inductance	51.54 μH
R_{loss}	Pad resistance at 38.4 kHz	81.6 mΩ
I_1	Primary current	20 A
OD$_1$	Main coil outer diameter	500 mm
OD$_c$	Cancelation coil outer diameter	500 mm
ID$_1$	Main coil inner diameter	357.2 mm
ID$_c$	Cancelation coil inner diameter	357.2 mm
C_{w}	Copper winding width	71.4 mm
h	Main–Cancelation coil distance	100 mm
N_1	Main coil number of turns	9
N_c	Cancelation coil number of turns	3

as follows:

$$L_{ii} \simeq \mu_0 \rho_i \left[\log\left(\frac{4\rho_i}{d_i}\right) - 1.75 \right]. \tag{9}$$

Consequently, the self-inductance of a coil of n closed-loop turns of radii ρ_i can be found by the addition of the mutual inductance between each pair of spiral turns in (8) and the self-inductance in (9) as

$$L = \sum_{i=1}^{n} L_{ii} + \sum_{i=1}^{n} \sum_{j=1, j\neq i}^{n} M_{ij}. \tag{10}$$

Equations (8) and (9) can be used to find the self-inductances and mutual inductance of a CNFP without a secondary pad. Fig. 3(a) shows the equivalent electrical circuit diagram in which the main and cancelation coils are connected in a series-opposing configuration. The equivalent inductance of such a configuration can be found as $L_{\text{eq}} = L_1 + L_c - 2M$, where M is the mutual inductance between L_1 and L_c. Fig. 3(b) shows a plot of the self-inductances L_1, L_c, mutual inductance M, and the equivalent inductance L_{eq} of a CNFP pad for different values of the distance h between the coils. Notice that for $h = 100$ mm, the value of the equivalent inductance is nearly 50 μH which, as shown in Table I, closely matches that of the physical system.

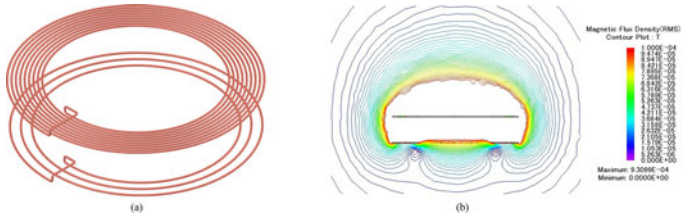

Fig. 4. Three-dimensional depiction of the CNFP pad. (a) 3-D CAD model used for FEM analysis. The coils are series connected (not shown here). (b) Contour plot (isolines) of the magnetic flux density driven with a primary current $I_1 = 20$ A.

IV. CIRCULAR NONFERRITE PAD

A CNFP, as proposed here, uses two annular coils with a primary coil of outer diameter OD$_1$, inner diameter ID$_1$ with evenly distributed N_1 turns and a cancelation coil of outer diameter OD$_c$, inner diameter ID$_c$, and N_c turns located under the primary coil at a distance h, as shown in Fig. 2(a). Both coils are wound with one single wire in a series-opposing configuration to generate opposing magnetic fields, thus $I_c = -I_1$.

Fig. 4(a) shows a three-dimensional (3-D) model of the proposed pad, while Fig. 4(b) shows a 2-D cross-sectional flux plot. For simplicity, it is assumed that both coils have the same inner and outer diameters but can have different numbers of turns N_1 and N_c. Equation (3) can be used to find a suitable turns ratio

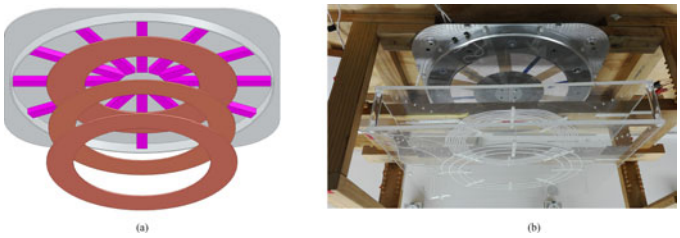

Fig. 5. CAD and experimental setup of the CNFP and CP pair. (a) 3-D depiction of the CNFP to CP pads. (b) Lab setup of the experiments.

N_1/N_c for a good front-to-back flux ratio. Fig. 2(b) shows the z component of the magnetic flux field, $|B_z|$, for different values of N_c with $\text{OD}_1 = \text{OD}_c = 500$ mm, $\text{ID}_1 = \text{ID}_c = 357.2$ mm, $h = 200$ mm, and $N_1 = 9$. The turns in each coil were evenly distributed between the inner and outer diameter ID_i and OD_i, respectively. For practical matters, the numbers of turns are chosen to be integer numbers, as each turn must return to the start point to be fed by the power supply. It can be observed that a ratio of $N_1/N_c \approx 3$ is a good choice with the flux falling rapidly below the ICNIRP limit of 27 μT [24] required for human interaction in less than 100 mm and approaching zero below the cancelation coil.

Although the magnitude of the field for the $N_1/N_c = 3$ ratio is slightly smaller than that of a single coil (B_1 only), at high air gaps (200 mm above main coil), the difference is small while the flux out the back of the pad is significantly reduced. This turns ratio is optimal for the specific parameters chosen for this pad. However, if the diameter of either coil, the distance between the two coils h, or the distance between each consecutive turn in the loop coil is changed, a new optimal turns ratio may be necessary to produce significantly more flux out the top of the pad and essentially no flux below the cancelation coil. For this study, h was fixed such that the mutual inductance between the two is just enough to provide good cancelation and low impact on the coupling factors. Having a large distance between the main and cancelation coils decreases its ability to reduce stray magnetic fields as the pad approaches a single air coil.

A laboratory prototype of the CNFP pad was built to validate the initial design simulations. Fig. 5(a) shows a depiction of the 3-D CAD model used to carry out the FEM simulations. The dimensions and parameters of the CNFP pad are described in Table I. Here, OD and ID are the outer and inner diameter, respectively, h is the distance between the main coil and the cancelation coil, and N_1 and N_c are the numbers of turns of the main and cancelation coils, respectively. A circular ferrite pad (CP), as described in [18], was used as a secondary pad. The secondary CP pad has a coil diameter of 500 mm with $N = 25$ turns and overall pad size (aluminum shield) of 722 mm $\times$ 722 mm. Fig. 5(b) shows a photo of the experimental setup of the pads. The primary pad was driven with a current $I_{\text{peak}} = 20$ A and an operating frequency $f = 38.4$ kHz. Coupling factors were measured and simulated for different z values and displacements of the secondary pad, and the results are shown in Fig. 6. The simulated and measured values here are within 2% of each other and are within the acceptable range of values for efficient power transfer [2].

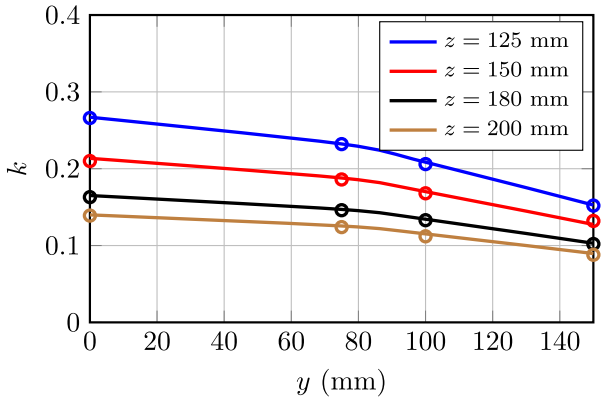

Fig. 6. CNFP to CP coupling factor measurements and simulation validation for different secondary pad air gaps z and displacements x. Solid lines represent simulated data; circles correspond to lab measurements.

V. Optimization

A key parameter in the design of high-power IPT systems is the maximum achievable power before reaching the ICNIRP limit of 27 μT, or the power-to-leakage flux ratio. Stray magnetic fields must be contained inside the charging region as much as possible to prevent them from reaching people standing near the charging pads. Fig. 7 illustrates the 3-D CAD setup used to investigate the effect that changing the diameter of the cancelation coil has on both the coupling factors and leakage flux using FEM simulations. Parallel test planes were used to measure the maximum rms flux density at 850 mm from the center of the secondary pad along the direction of displacement. These test planes constitute dummy elements with the physical properties of air and, as shown, are denominated "left" and "right" test planes, respectively. The left test plane is placed on the opposite side of the secondary displacement ($-y$), while the right test plane is on the same side of the secondary displacement ($+y$). The planes were fixed relative to the secondary pad so as to simulate the outer boundaries of the chassis of a car.

Fig. 8(a) shows that the change in coupling factors as the outer diameter of the cancelation coil OD_c is varied from 500 to 750 mm. The inner diameter ID_c was changed accordingly to keep the winding width C_w constant. The tendency is for the coupling to decrease with increasing values of OD_c, however, the change is very small, as seen from the low slope of the lines in Fig. 8(a). An interesting finding is the effect this change has on the flux leakage outside the charging region. Fig. 8(b) shows how the magnetic flux leakage decreases as the diameter of the cancelation coil OD_c is increased for a secondary displaced $y = 150$ mm. It can be seen that a good compromise between coupling and leakage can be achieved for OD_c from 655 to 670 mm, as the reduction in coupling is minimal while the leakage flux is near a minimum value.

The effect that the separation between the main and cancelation coils h has on several important parameters is shown in Fig. 9. The change in coupling factors as h is increased is shown to be insignificant. However, the uncompensated apparent power at the secondary P_{su} tends to increase slightly with increasing h, as seen in Fig. 9(a). This increase in P_{su} is mainly

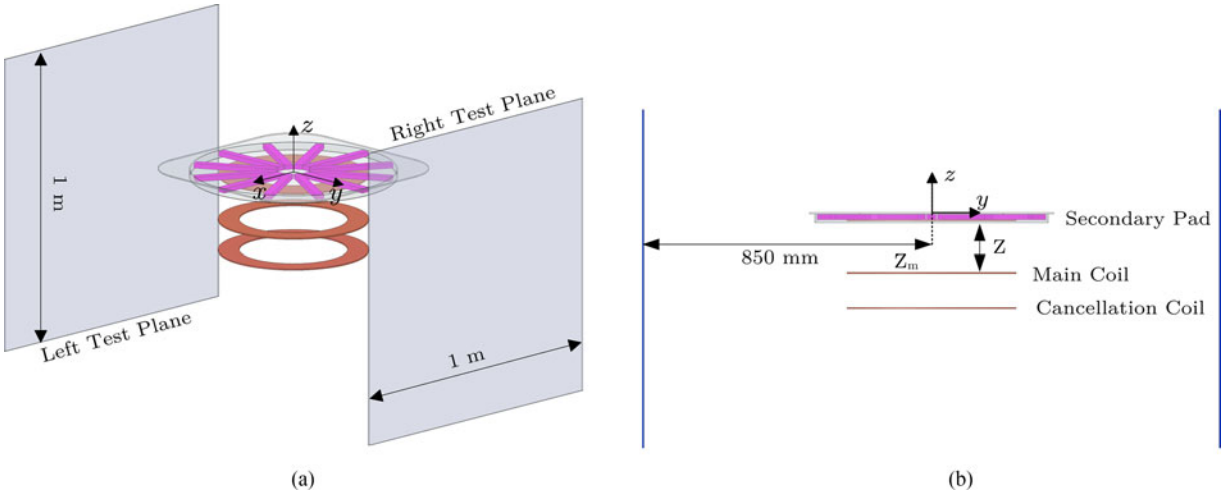

Fig. 7. Simulation model setup of a CP on CNFP with leakage flux test measurement planes. (a) Perspective view with test planes. (b) Front view.

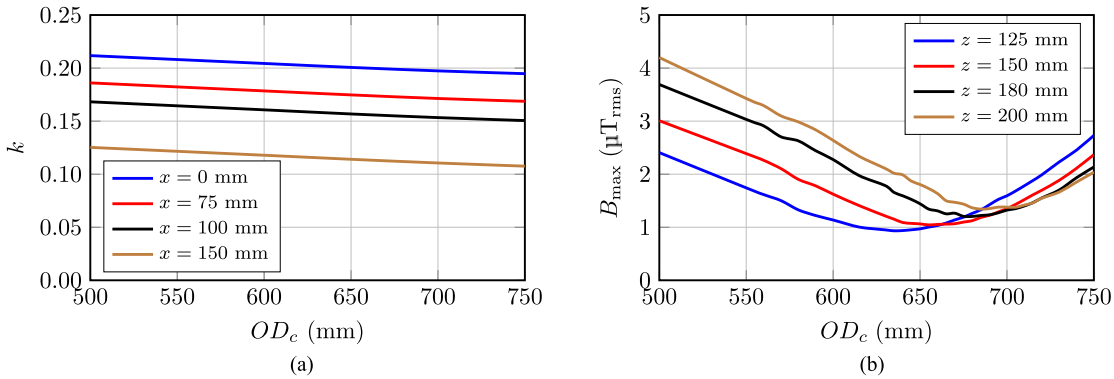

Fig. 8. Coupling factors and maximum rms leakage flux plots for a CP on CNFP pair. Flux measured on the left test plane at 850mm from the center of the secondary. (a) Coupling factors. (b) Leakage flux for secondary offset $x = 150$ mm with respect to the primary.

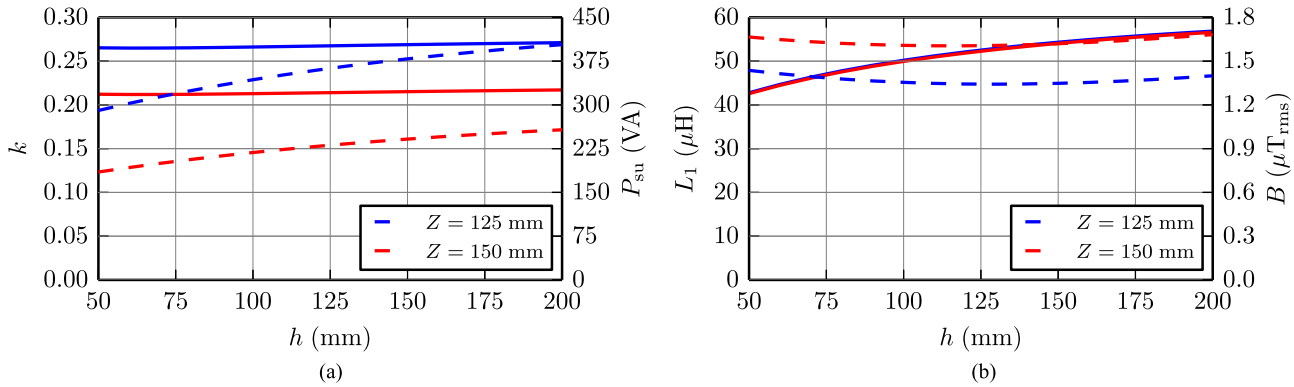

Fig. 9. Effect of separation (h) between the main and cancelation coils at two separate air gaps. (a) k (solid lines) and $P_{\rm su}$ (dashed lines). (b) L_1 (solid lines) and $B_{\rm rms}$ (dashed lines) measured at $(0, 800, \text{Z}/2)$ mm. The primary current was $I_{1,\rm peak} = 20$ A while $\text{OD}_c = 500$ mm.

due to the change in the total inductance of the CNFP as depicted in Fig. 9(b). The closer the main and cancelation coils are, the higher the mutual inductance between them. Hence, the total inductance of the pad will be smaller due to the series-opposing configuration of these two coils. The stray magnetic field is shown to be measured at the middle point between the primary and secondary pads 800 mm in the y-direction, which falls very close to where the maximum leakage flux is. The stray magnetic field slightly dips for 100 rm mm $\leq h \leq 140$ mm, as shown in Fig. 9(b). Choosing an appropriate distance h between the coils is a tradeoff between the achievable output power transfer level, and stray magnetic field emissions, as well as size. In

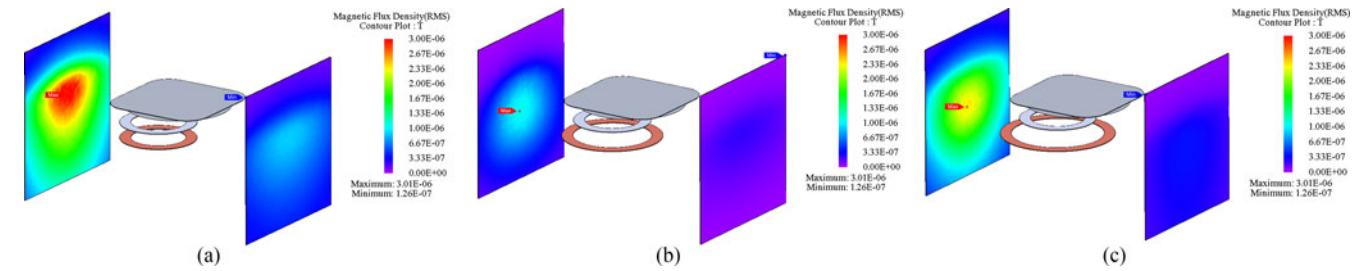

Fig. 10. Flux leakage contour plots for a CP on CNFP for different cancelation coil diameters at a $z = 150$ mm air gap and $X = 150$ mm displacement. (a) $\mathrm{OD}_c = 500$ mm. (b) $\mathrm{OD}_c = 650$ mm. (c) $\mathrm{OD}_c = 750$ mm.

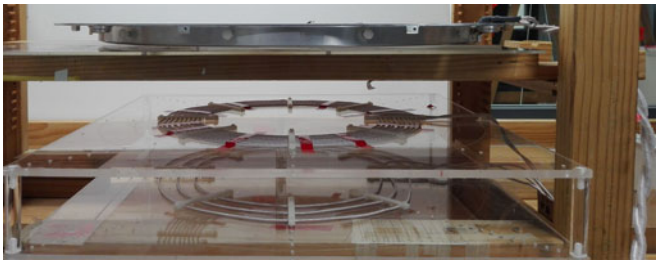

Fig. 11. Experimental setup of CNFP to CP pads.

this study, the separation was chosen to be $h = 100$ mm as a suitable compromise between both and provides a primary pad with the required impedance for the available lab power supply (no extra compensation capacitor is required). Also, this height has been implemented in other systems [14], [59] and having some depth in a primary side system is an advantage in ground installation for added robustness.

Fig. 10 shows a flux contour plot to visually reinforce the change in flux leakage as the cancelation coil diameter is swept from 500 to 750 mm. The secondary pad was kept at an air gap $z = 150$ mm and offset $y = 150$ mm. It is clear that a significant drop in emissions at the test planes is achieved. In addition, it shows that the region of interest for flux reduction is opposite the direction of travel of the secondary pad, which would be more exposed due to the misaligned pads. In this case, it is the left test plane, as that is where the leakage flux is of high intensity. Therefore, flux leakage measurements are only done on this side of the pads hereafter.

VI. Experimental Validation and Comparison

Laboratory scale prototypes were built for validating the simulated CAD models. Fig. 11 shows the setup of the CNFP on CP prototypes. Measurement of the magnetic flux leakage was done using a NARDA ELT-400 probe located 800 mm from the center of the secondary pad at the middle air gap point; a high precision *LCR* meter (Agilent E4940A) was used to measure inductances and coupling factors at small-signal levels, while the YOKOGAWA WT1800 power meter was used to measure the currents and voltages across the pads at high signal levels. Fig. 12 shows the measured and simulated rms magnetic flux density. The measured data are in excellent agreement with the simulated results, confirming the validity of the FEM models. The CP–CP pair has the lowest emissions, while the "air coil"

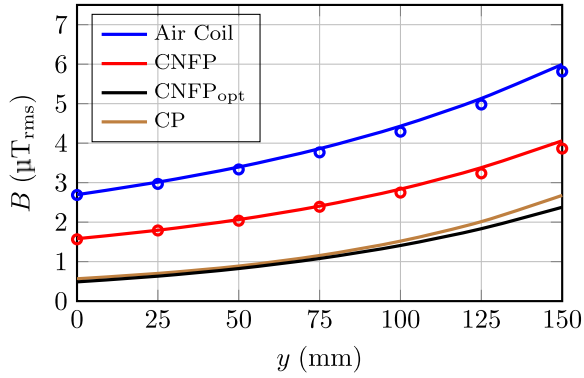

Fig. 12. Magnetic flux density validation for the CNFP, CP, and air coil primaries coupled to a CP secondary. The measurement point $P_{\mathrm{test}}(x, y, z)$ was chosen at 800 mm from the center of the secondary at the midpoint of the air gap $P_{\mathrm{test}}(x, y, z) = (0, 800, 75)$ mm and the input current $I_{1,\mathrm{peak}} = 20$ A. The optimized version of the CNFP (CNFP$_{\mathrm{opt}}$) has been added for comparison. (Solid lines represent simulated data whereas the circles represent the measured points).

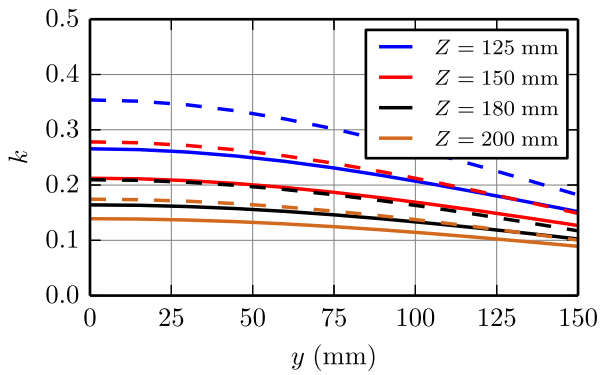

Fig. 13. Coupling factors comparison for the CNFP and CP at different air gaps as the secondary pad is displaced. Solid lines correspond to the CNFP while dashed lines correspond to the CP primary.

was found to have the highest leakage flux outside the charging region. The CNFP, before optimization, has a higher leakage flux than that of a CP. However, as shown in Fig. 12, when a cancelation coil with a diameter $\mathrm{OD}_c = 660$ mm is used, the leakage flux of the CNFP matches that of the CP. Fig. 13 shows a plot of the coupling factors for both the CNFP and CP primaries at different air gaps as the secondary pad is displaced along the x-direction. The CP exhibits higher coupling factors than the CNFP; however, the change in coupling factors as the

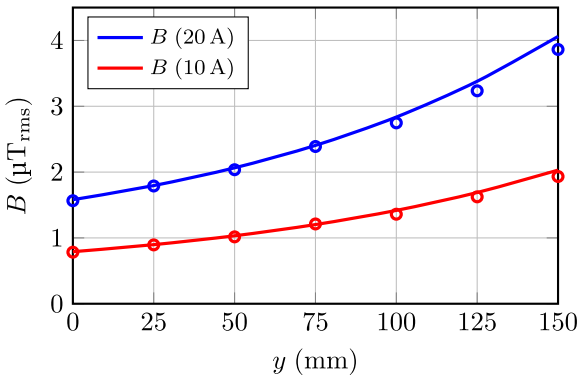

Fig. 14. Magnetic flux density for CNFP–CP pair measured/simulated at a test point 800 mm from the center of the secondary pad at a midpoint air gap $P_{\text{test}}(x, y, z) = (0, 800, 75)$ mm for primary currents $I_{1,\text{peak}} = 10$ A and $I_{1,\text{peak}} = 20$ A. (Circles represent measured points, while solid lines correspond to FEM simulation).

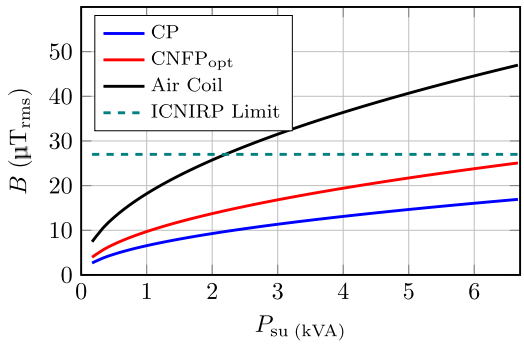

Fig. 15. Comparison between the leakage flux as a function of the required output power for the CNFP, CP, and air coil primary pads against the ICNIRP 27 μT limit. The secondary pad was placed at an offset $X = 150$ mm and an air gap of $Z = 150$ mm for a test point 800mm from the center of the secondary and midpoint air gap $P_{\text{test}}(x, y, z) = (0, 800, 75)$ mm.

secondary is displaced is less pronounced for the CNFP, especially at higher air gaps. Also, even though the coupling factors are smaller, they fall in the range required for efficient power transfer [2].

As seen in (3), the magnetic field is directly proportional to the amp-turns or NI of the coil. This relationship is especially true for coils in air. However, for ferrite pads, the system can be considered almost totally linear as long as the ferrite is kept out of the saturation region. Ferrite losses are more complicated as other nonlinear dependencies arise such as temperature and frequency. For the sake of simplicity, in this paper, the frequency is fixed at 38.4 kHz and the effects of temperature are neglected. All systems in this paper are assumed to be linear, as care has been taken not to saturate the ferrite and to fix the operating frequency at 38.4 kHz. Fig. 14 depicts the magnetic fields, both measured and simulated, for two different primary currents, $I_1 = 10$ and 20 A, respectively. It shows that by doubling the primary current, the magnetic field is also doubled; hence, the ratio $B(20\text{ A})/B(10\text{ A})$ in Fig. 14 between the two is constant regardless of the secondary pad displacement, which further confirms that this IPT system is linear.

Even though the CNFP can be optimized to produce a reduction in leakage flux, it also suffers a reduction in coupling factors and, in consequence, the output power. A comparison in terms of "power per leakage" is required between the investigated pads to better assess their power transfer capability. Power per leakage measures the amount of power a pad can transfer versus the pad's stray field emissions. Pads that can transfer more power with less stray leakage are preferable. In order to compare the different primary pads, the uncompensated apparent power P_{su} in the secondary pad was kept constant with an unloaded secondary so that it does not impact the flux provided by the primary pad under test. The required output power was assumed to be provided only from the primary pad by generating the appropriate VA. The required input current necessary to produce the required uncompensated power can be determined from (2).

Fig. 15 shows the rms leakage flux for a range of uncompensated output powers for the CNFP, CP, and air coil primary pads. Notice that the CNFP can provide high amounts of power before reaching the ICNIRP 27 μT limit. For this comparison, all pads used identical coils in the primary pad, i.e., same volume and surface area of copper, and the same number of turns. Even though the CNFP has slightly worse performance than the CP in terms of power per leakage, the CNFP will not incur core or eddy current losses as it does not use any ferrite or aluminum. Relative core losses in the ferrite can become significant at high power and the potential for thermal runaway also increases. Furthermore, ferrite and aluminum can be expensive, increasing the overall system's cost. These considerations make the CNFP a potentially cost-effective alternative for roadway IPT applications.

It is worth pointing out that the overall dimension of the CP ferrite-based pad is much bigger than that of the optimized version of the CNFP. The aluminum back plate is not used in the CNFP design, but is usually present in ferrite-based pads to remove stray leakage. In the case of the ferrite pad used here for the comparative analysis, this aluminum back plate was $710 \times 710\,\text{mm}^2$. In contrast, the maximum diameter of the cancelation coil in the optimized CNFP presented was $660\,\text{mm}^2$. Therefore, there is considerable scope to increase the diameter of this CNFP design to improve the coupling and power transfer to the secondary, particularly under misaligned conditions, and further improve the power output while maintaining a low leakage footprint. The analysis presented in this paper can be applied to smaller or larger systems as the superposition principle allows the system to be scaled. However, care must be taken as the best turns ratio between the main and cancelation coils can change when the relative dimensions of both coils change.

Roadways are traditionally built out of concrete, bitumen, or asphalt, and reinforcing materials, such as steel rebars, are commonly used. Fig. 16 illustrates the effect that a $750 \times 570 \times 1.5\,\text{mm}^3$ steel sheet placed at different distances D_{steel} behind the cancelation coil has on the primary inductance and ac resistance (losses). The change in inductance is below 2.6% and can be considered negligible. As the pad resistance and, thus, the losses, increases, the closer the steel sheet is to the pad by as much as 20 per cent. However, the resistance is still small. In practice, a coarse mesh of rebars is used for concrete reinforcement. Therefore, the effect of such meshes in the proximity of

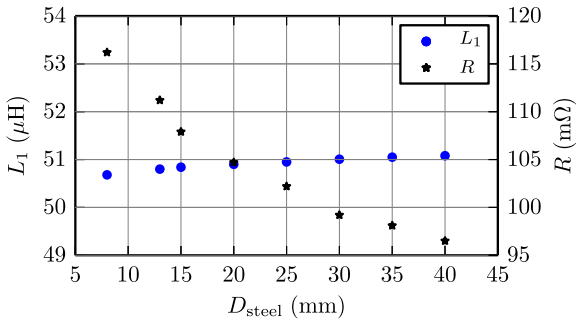

Fig. 16. Measurements of primary inductance and ac resistance as a function of the distance between a 750 × 570 × 1.5 mm^3 steel sheet and the cancelation coil. Primary inductance and resistance without the steel sheet present are 51.208 μH and 80.5 mΩ, respectively.

the pad is expected to be much smaller than that of the steel sheet shown in Fig. 16. Both glass and concrete are nonmagnetic materials and their magnetic permeability is similar to the permeability of free space [60]. Therefore, fiberglass reinforced concrete could be used to enhance the strength of any concrete without impacting the performance of the IPT system.

VII. Conclusion

This paper introduced a circular-shaped ferrite-less pad, called CNFP, suitable for high-power EV roadway charging applications. The pad is comprised of two series-connected coils positioned vertically with the bottom coil designed to reduce flux leakage. This topology is able to produce a single-sided flux without using ferrimagnetic material to shape the magnetic field. In conventional measures of the performance of wireless charging pads, i.e., coupling factor and leakage flux, the pad has a performance within the acceptable ranges while being physically robust, and suitable for harsh environments. The absence of ferrite gives the pad the ability to be overdriven for short periods of time, which would be useful for a roadway dynamic charging system. It was shown that this pad can achieve coupling factors within the range for efficient wireless power transfer. Furthermore, by carefully balancing the amp-turns or NI ratio between the main and cancelation coils, the leakage fluxes out the bottom and sides of the charging region have been significantly reduced. This feature is highly desired as the power can be increased by boosting the primary VA without exceeding the emissions limit. It was also shown that looking at just the shielding effectiveness of a cancelation technique is not enough when assessing the power transfer capability of an IPT system. Parameters such as coupling factors and power-per-leakage must be taken into account.

The work presented in this paper aims to demonstrate some unique features of the CNFP that can be useful for roadway charging environments. Because of its lack of aluminum, plastic, or ferrite, the CNFP is more physically rugged than other pads, can be better integrated into roadway environments, and requires less protection cover over the upper surface of the roadway, potentially making the effective air gap smaller than that of pads needing more protective materials. The diameter of the coils can also be larger to closely match the size of ferrite-based pads using larger aluminum back planes, thereby increasing the coupling factors. Further research must be undertaken to investigate the overall efficiency of a high-power prototype and compare it to a similar ferrite pad including losses in the core and aluminum shield.

References

[1] A. W. Green and J. T. Boys, "A 10 kHz inductively coupled power transfer-concept and control," in *Proc. 5th Int. Conf. Power Electron. Variable-Speed Drives*, 1994, pp. 694–699.
[2] J. Boys, G. Covic, and A. Green, "Stability and control of inductively coupled power transfer systems," *Inst. Elect. Eng. Proc., Electr. Power Appl.*, vol. 147, no. 1, pp. 37–43, Jan. 2000.
[3] G. A. J. Elliott, G. A. Covic, D. Kacprzak, and J. T. Boys, "A new concept: Asymmetrical pick-ups for inductively coupled power transfer monorail systems," *IEEE Trans. Magn.*, vol. 42, no. 10, pp. 3389–3391, Oct. 2006.
[4] G. A. Covic and J. T. Boys, "Inductive power transfer," *Proc. IEEE*, vol. 101, no. 6, pp. 1276–1289, Jun. 2013.
[5] J. Sallan, J. Villa, A. Llombart, and J. Sanz, "Optimal design of ICPT systems applied to electric vehicle battery charge," *IEEE Trans. Ind. Electron.*, vol. 56, no. 6, pp. 2140–2149, Jun. 2009.
[6] J. Shin *et al.*, "Design and implementation of shaped magnetic-resonance-based wireless power transfer system for roadway-powered moving electric vehicles," *IEEE Trans. Ind. Electron.*, vol. 61, no. 3, pp. 1179–1192, Mar. 2014.
[7] Z. Cong *et al.*, "High-efficiency contactless power transfer system for electric vehicle battery charging application," *IEEE J. Emerg. Sel. Topics Power Electron.*, vol. 3, no. 1, pp. 65–74, Mar. 2015.
[8] B. Lenaerts and R. Puers, *Omnidirectional Inductive Powering for Biomedical Implants*, 1st ed. Delft, The Netherlands: Springer-Verlag, 2009.
[9] S. H. Song, A. Kim, and B. Ziaie, "Omnidirectional ultrasonic powering for millimeter-scale implantable devices," *IEEE Trans. Biomed. Eng.*, vol. 62, no. 11, pp. 2717–2723, Nov. 2015.
[10] B. H. Choi, V. X. Thai, E. S. Lee, J. H. Kim, and C. T. Rim, "Dipole-coil-based wide-range inductive power transfer systems for wireless sensors," *IEEE Trans. Ind. Electron.*, vol. 63, no. 5, pp. 3158–3167, May 2016.
[11] G. A. Covic and J. T. Boys, "Modern trends in inductive power transfer for transportation applications," *J. Emerg. Sel. Topics Power Electron.*, vol. 1, no. 1, pp. 28–41, Mar. 2013.
[12] S. Li and C. C. Mi, "Wireless power transfer for electric vehicle applications," *IEEE J. Emerg. Sel. Topics Power Electron.*, vol. 3, no. 1, pp. 4–17, Mar. 2015.
[13] S. Y. R. Hui, W. Zhong, and C. K. Lee, "A critical review of recent progress in mid-range wireless power transfer," *IEEE Trans. Power Electron.*, vol. 29, no. 9, pp. 4500–4511, Sep. 2014.
[14] J. Huh, S. W. Lee, W. Y. Lee, G. H. Cho, and C. T. Rim, "Narrow-width inductive power transfer system for online electrical vehicles," *IEEE Trans. Power Electron.*, vol. 26, no. 12, pp. 3666–3679, Dec. 2011.
[15] C. Park, S. Lee, G.-H. Cho, and C. T. Rim, "Innovative 5-m-off-distance inductive power transfer systems with optimally shaped dipole coils," *IEEE Trans. Power Electron.*, vol. 30, no. 2, pp. 817–827, Feb. 2015.
[16] C. Park, S. Lee, S. Y. Jeong, G.-H. Cho, and C. T. Rim, "Uniform power I-type inductive power transfer system with DQ power supply rails for on-line electric vehicles," *IEEE Trans. Power Electron.*, vol. 30, no. 11, pp. 6446–6455, Nov. 2015.
[17] M. Budhia, G. Covic, and J. Boys, "A new IPT magnetic coupler for electric vehicle charging systems," in *Proc. 36th Annu. Conf. IEEE Ind. Electron. Soc.*, 2010, pp. 2487–2492.
[18] M. Budhia, G. A. Covic, and J. T. Boys, "Design and optimization of circular magnetic structures for lumped inductive power transfer systems," *IEEE Trans. Power Electron.*, vol. 26, no. 11, pp. 3096–3108, Nov. 2011.
[19] M. Budhia, J. T. Boys, and G. A. Covic, "Development of a single-sided flux magnetic coupler for electric vehicle IPT charging systems," *IEEE Trans. Ind. Electron.*, vol. 60, no. 1, pp. 318–328, Jan. 2013.
[20] A. Zaheer, H. Hao, G. A. Covic, and D. Kacprzak, "Investigation of multiple decoupled coil primary pad topologies in lumped IPT systems for interoperable electric vehicle charging," *IEEE Trans. Power Electron.*, vol. 30, no. 4, pp. 1937–1955, Apr. 2015.
[21] I. Fujita, T. Yamanaka, Y. Kaneko, S. Abe, and T. Yasuda, "A 10 kW transformer with a novel cooling structure of a contactless power transfer

system for electric vehicles," in *Proc. IEEE Energy Convers. Congr. Expo.*, Sep. 2013, pp. 3643–3650.
[22] S. Kim, A. Zaheer, G. Covic, and J. Boys, "Tripolar pad for inductive power transfer systems," in *Proc. 40th Annu. Conf. IEEE Ind. Electron. Soc.*, Oct. 2014, pp. 3066–3072.
[23] S. Y. Choi, S. Y. Jeong, E. S. Lee, B. W. Gu, S. W. Lee, and C. T. Rim, "Generalized models on self-decoupled dual pick-up coils for large lateral tolerance," *IEEE Trans. Power Electron.*, vol. 30, no. 11, pp. 6434–6445, Nov. 2015.
[24] ICNIRP, "Guidelines for limiting exposure to time-varying electric and magnetic fields (1 Hz to 100 kHz)," *Health Phys.*, vol. 99, no. 6, pp. 818–836, Dec. 2010.
[25] A. Christ *et al.*, "Evaluation of wireless resonant power transfer systems with human electromagnetic exposure limits," *IEEE Trans. Electromagn. Compat.*, vol. 55, no. 2, pp. 265–274, Apr. 2013.
[26] P. P. Ding, L. Bernard, L. Pichon, and A. Razek, "Evaluation of electromagnetic fields in human body exposed to wireless inductive charging system," *IEEE Trans. Magn.*, vol. 50, no. 2, pp. 1037–1040, Feb. 2014.
[27] H. Moon, S. Kim, H. H. Park, and S. Ahn, "Design of a resonant reactive shield with double coils and a phase shifter for wireless charging of electric vehicles," *IEEE Trans. Magn.*, vol. 51, no. 3, Mar. 2015, Art. no. 8700104.
[28] M. Feliziani and S. Cruciani, "Mitigation of the magnetic field generated by a wireless power transfer (WPT) system without reducing the WPT efficiency," in *Proc. Int. Symp. Electromagn. Compat.*, Sep. 2013, pp. 610–615.
[29] S. Cruciani, T. Campi, M. Feliziani, and F. Maradei, "Optimum coil configuration of wireless power transfer system in presence of shields," in *Proc. IEEE Int. Symp. Electromagn. Compat.*, 2015, pp. 720–725.
[30] A. E. Umenei, J. Schwannecke, S. Velpula, and D. Baarman, "Novel method for selective nonlinear flux guide switching for contactless inductive power transfer," *IEEE Trans. Magn.*, vol. 48, no. 7, pp. 2192–2195, Jul. 2012.
[31] E. Waffenschmidt and T. Staring, "Limitation of inductive power transfer for consumer applications," in *Proc. 13th Eur. Conf. Power Electron. Appl.*, Sep. 2009, pp. 1–10.
[32] S. Ahn *et al.*, "Low frequency electromagnetic field reduction techniques for the on-line electric vehicle (OLEV)," in *Proc. IEEE Int. Symp. Electromagn. Compat.*, 2010, pp. 625–630.
[33] H. Kim, C. Song, and J. Kim, "Coil design for high efficiency and low magnetic field leakage of wireless charging system for electric vehicle," in *Proc. Wireless Power Transfer Conf.*, 2015, pp. 1–3.
[34] H. Kim, C. Song, D. H. Kim, and J. Kim, "Design of conductive shield for wireless power transfer system for electric vehicle considering automotive body," in *Proc. 2015 IEEE Int. Symp. Electromagn. Compat.*, 2015, pp. 1369–1374.
[35] H. Kim, J. Cho, S. Ahn, J. Kim, and J. Kim, "Suppression of leakage magnetic field from a wireless power transfer system using ferrimagnetic material and metallic shielding," in *Proc. IEEE Int. Symp. Electromagn. Compat.*, 2012, pp. 640–645.
[36] J. Kim *et al.*, "Coil design and shielding methods for a magnetic resonant wireless power transfer system," *Proc. IEEE*, vol. 101, no. 6, pp. 1332–1342, Jun. 2013.
[37] S. Kim, H. H. Park, J. Kim, J. Kim, and S. Ahn, "Design and analysis of a resonant reactive shield for a wireless power electric vehicle," *IEEE Trans. Microw. Theory Techn.*, vol. 62, no. 4, pp. 1057–1066, Apr. 2014.
[38] S. Y. Choi, B. W. Gu, S. W. Lee, W. Y. Lee, J. Huh, and C. T. Rim, "Generalized active EMF cancel methods for wireless electric vehicles," *IEEE Trans. Power Electron.*, vol. 29, no. 11, pp. 5770–5783, Nov. 2014.
[39] V. Prasanth and P. Bauer, "Distributed IPT systems for dynamic powering: Misalignment analysis," *IEEE Trans. Ind. Electron.*, vol. 61, no. 11, pp. 6013–6021, Nov. 2014.
[40] R. Bosshard, J. W. Kolar, J. Mühlethaler, I. Stevanović, B. Wunsch, and F. Canales, "Modeling and η-α-pareto optimization of inductive power transfer coils for electric vehicles," *IEEE J. Emerg. Sel. Topics Power Electron.*, vol. 3, no. 1, pp. 50–64, Mar. 2015.
[41] F. Lu, H. Zhang, H. Hofmann, and C. Mi, "A high efficiency 3.3 kW loosely-coupled wireless power transfer system without magnetic material," in *Proc. IEEE Energy Convers. Congr. Expo.*, 2015, pp. 2282–2286.
[42] A. Tejeda, G. A. Covic, and J. T. Boys, "Novel single-sided ferrite-less magnetic coupler for roadway EV charging," in *Proc. IEEE Energy Convers. Congr. Expo.*, 2015, pp. 3148–3153.
[43] Y. H. Sohn, B. H. Choi, E. S. Lee, and C. T. Rim, "Comparisons of magnetic field shaping methods for ubiquitous wireless power transfer," in *Proc. IEEE PELS Workshop Emerg. Technol., Wireless Power*, 2015, pp. 1–6.
[44] E. Noh, K. H. Ko, and K. Kim, "Transmitter coil system without ferrite in wireless power transfer," *Electron. Lett.*, vol. 52, no. 5, pp. 392–393, Mar. 2016.
[45] S. Lee, S. Ahn, and I. Jang, "Simulation-based feasibility study on the wireless charging railway system with a ferriteless primary module," *IEEE Trans. Veh. Technol.*, 2016, to be published.
[46] J. T. Boys, G. A. Covic, A. Tejeda, M. Pierce, and J. Gawith, "Magnetic flux coupling structures with controlled flux cancellation," Patent WO 039 644 A2, Mar. 17, 2016.
[47] R. Basar, M. Y. Ahmad, J. Cho, and F. Ibrahim, "Application of wireless power transmission systems in wireless capsule endoscopy: An overview," *Sensors*, vol. 14, no. 6, pp. 10 929–10 951, 2014.
[48] W. Xin, G. Yan, and W. Wang, "Study of a wireless power transmission system for an active capsule endoscope," *Int. J. Med. Robot. Comput. Assisted Surg.*, vol. 6, no. 1, pp. 113–122, Jan. 2010.
[49] G. Tortora, F. Mulana, G. Ciuti, P. Dario, and A. Menciassi, "Inductive-based wireless power recharging system for an innovative endoscopic capsule," *Energies*, vol. 8, pp. 10 315–10 334, 2015.
[50] A. F. R. Alvarez, E. Franco-Mejia, and C. R. Pinedo-Jaramillo, "Study and analysis of magnetic field homogeneity of square and circular Helmholtz coil pairs: A Taylor series approximation," in *Proc. Andean Region Int. Conf.*, 2012, pp. 77–80.
[51] V. E. Baranova and P. F. Baranov, "The Helmholtz coils simulating and improved in COMSOL," in *Proc. Dyn. Syst., Mech. Mach. (Dyn.)*, 2014, pp. 1–4.
[52] C. K. Lee, W. X. Zhong, and S. Y. R. Hui, "Effects of magnetic coupling of nonadjacent resonators on wireless power domino-resonator systems," *IEEE Trans. Power Electron.*, vol. 27, no. 4, pp. 1905–1916, Apr. 2012.
[53] W. X. Zhong, C. K. Lee, and S. Y. Hui, "Wireless power domino-resonator systems with noncoaxial axes and circular structures," *IEEE Trans. Power Electron.*, vol. 27, no. 11, pp. 4750–4762, Nov. 2012.
[54] F. W. Grover, *Inductance Calculations: Working Formulas and Tables*, 1st ed. New York, NY, USA: Dover, 2009.
[55] J. T. Conway, "Analytical and semi-analytical solutions for the force between circular loops in parallel planes," *IEEE Trans. Magn.*, vol. 49, no. 8, pp. 4817–4823, Aug. 2013.
[56] J. A. Stratton, *Electromagnetic Theory*. New York, NY, USA: McGraw-Hill, 1941.
[57] Y. Su, X. Liu, and S. Hui, "Mutual inductance calculation of movable planar coils on parallel surfaces," *IEEE Trans. Power Electron.*, vol. 24, no. 4, pp. 1115–1123, Apr. 2009.
[58] W. Hurley and M. Duffy, "Calculation of self and mutual impedances in planar magnetic structures," *IEEE Trans. Magn.*, vol. 31, no. 4, pp. 2416–2422, Jul. 1995.
[59] C. C. Mi, G. Buja, S. Y. Choi, and C. T. Rim, "Modern advances in wireless power transfer systems for roadway powered electric vehicles," *IEEE Trans. Ind. Electron.*, vol. 63, no. 10, pp. 6533–6545, Oct. 2016.
[60] H. C. Rim and O. Buyukozturk, "Electromagnetic properties of concrete at microwave frequency range," *ACI Mater. J.*, vol. 95, no. 3, pp. 262–271, May 1998.

Abiezer Tejeda (S'10–M'14) received the B.Sc. and M.Sc. degrees in electrical and computer engineering from Utah State University, Logan, UT, USA, in 2010 and 2012, respectively. He is currently working toward the Ph.D. degree at The University of Auckland, Auckland, New Zealand.

His research interests include electromagnetic modeling and design of wireless power transfer systems with emphasis on electric vehicles charging applications.

Claudio Carretero (S'08–M'11–SM'15) received the B.Sc. and M.Sc. degrees in physics, the B.Sc. and M.Sc. degrees in electrical engineering, and the Ph.D. degree in electrical engineering from the University of Zaragoza, Zaragoza, Spain, in 1998, 2002 and 2010, respectively.

He is currently an Assistant Professor in the Department of Applied Physics, University of Zaragoza. His research interests include induction heating applications and electromagnetic modeling of inductive systems. He is a member of the Instituto de Investigación en Ingeniería de Aragón (I3A).

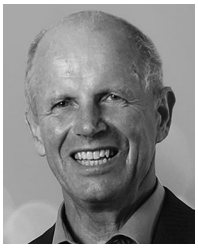

John T. Boys received the M.E. degree from the University of Auckland, Auckland, New Zealand, in 1965.

After completing the Ph.D. degree, he was with SPS technologies for five years before returning to academia as a Lecturer at the University of Canterbury. He moved to Auckland in 1977 where he developed his work in Power Electronics. He is currently a Distinguished Professor Emeritus at the University of Auckland in the Department of Electrical and Computer Engineering and a Cofounder of HaloIPT. He has published more than 100 papers in international journals and is the holder of more than 40 U.S. patents from which licenses in specialized application areas have been granted around the world. His specialist research areas include power electronics and electromagnetics for inductive power transfer, where he works with Prof. G. A. Covic.

Dr. Boys is a Fellow of the Royal Society of New Zealand and a Distinguished Fellow of the Institution of Professional Engineers New Zealand.

Grant A. Covic (S'88–M'89–SM'04) received the B.E. (Hons.) and Ph.D. degrees in electrical and electronic engineering from The University of Auckland (UoA), Auckland, New Zealand, in 1986 and 1993, respectively.

He was appointed as a full time Lecturer in 1992, a Senior Lecturer in 2000, an Associate Professor in 2007, and a Professor in 2013 within the Electrical and Computer Engineering Department, UoA. In 2010, he cofounded (with Prof. J. Boys) a new global start-up company HaloIPT focusing on electric vehicle (EV) wireless charging infrastructure, which was sold in late 2011. He presently heads inductive power research at the UoA and coleads the interoperability subteam within the SAE J2954 wireless charging standard for EVs. His research and consulting interests include power electronics, electric vehicle battery charging, and highly resonant inductive (contact-less) power transfer (IPT) in which he has published more than 100 refereed papers in international journals and conferences. He holds a number of U.S. patents with many more pending, from which licenses in specialized application areas of IPT have been granted around the world.

Dr. Covic is a Fellow of the Institution of Professional Engineers New Zealand, a Fellow of the Royal Society of New Zealand, and (together with Prof. Boys) received the New Zealand Prime Ministers Science Prize, the KiwiNet Research Commercialisation Award, and the Vice Chancellors Commercialisation Medal for his work in IPT.